Bulletin of the Seismological Society of America, Vol. 78, No. 4, pp. 1438–1449, August 1988

AFTERSHOCK PATTERNS AND MAIN SHOCK FAULTING

By Carlos Mendoza and Stephen H. Hartzell

Abstract

We have compared aftershock patterns following several moderate to large earthquakes with the corresponding distributions of coseismic slip obtained from previous analyses of the recorded strong ground motion and teleseismic waveforms. Well-located aftershock hypocenters are projected onto the main shock fault plane, and their positions are examined relative to the zones of coseismic displacement indicated by the estimated distributions of main shock slip. We also examine the aftershock focal mechanisms, when these data are available, in an attempt to identify possible patterns of secondary faulting within the aftershock zone.

Our results are consistent with a hypothesis of aftershock occurrence that requires a secondary redistribution of stress following primary failure on the earthquake fault. Aftershocks following the earthquakes examined in this study occur mostly outside of or near the edges of the source areas indicated by the patterns of main shock slip. The spatial distribution of aftershocks reflects either a continuation of slip in the outer regions of the areas of maximum coseismic displacement or the activation of subsidiary faults within the volume surrounding the boundaries of main shock rupture.

Introduction

Following a large earthquake, numerous aftershocks are usually observed to occur in the vicinity of the main shock hypocenter. Although the actual mechanics of aftershock generation are not well known, large earthquake ruptures seem to perturb the local stress field, sometimes resulting in complicated patterns of aftershock faulting. In some cases, these aftershocks appear to result from secondary deformation on preexisting subsidiary faults (e.g., King *et al.*, 1985; Savage and Meyer, 1985).

Few attempts have been made to compare the observed distribution of aftershock hypocenters following large earthquakes with patterns of coseismic displacement estimated from an analysis of the strong-motion and teleseismic records. Preliminary comparisons of the postseismic activity pattern with the estimated coseismic slip suggest that aftershocks do not occur where main shock slip is large. In one such comparison, Doser and Kanamori (1986) found that the aftershock activity following the 15 October 1979 Imperial Valley earthquake occurred outside of the region of high slip that Hartzell and Heaton (1983) obtained from an inversion of the strong-motion and teleseismic data. In a separate study, Hartzell and Heaton (1986) noted that aftershocks following the 24 April 1984 Morgan Hill earthquake occurred mostly outside of the areas of maximum slip estimated for the main shock following an inversion of the near-source strong-motion records. Figure 1 summarizes the comparisons of Doser and Kanamori (1986) and Hartzell and Heaton (1986) for the Imperial Valley and Morgan Hill earthquake sequences.

The results of these previous comparisons are consistent with the interpretation that aftershocks occur in regions where the stress level is high following

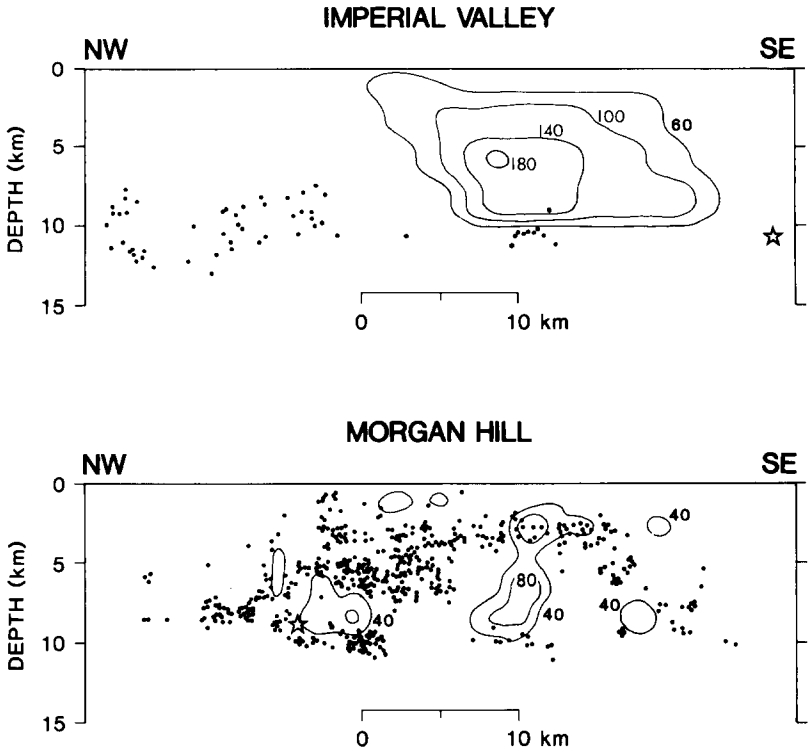

FIG. 1. Comparison of the aftershock distributions following the 1979 Imperial Valley (*top*) and the 1984 Morgan Hill (*bottom*) earthquakes with the corresponding distributions of main shock slip obtained by Hartzell and Heaton (1983, 1986). Strike-slip displacement is contoured at 40 cm intervals for both source models. The aftershock distribution shown for the Imperial Valley earthquake does not include additional aftershocks that occurred much farther to the north (from Doser and Kanamori, 1986). Morgan Hill aftershock locations are from Cockerham and Eaton (1987). Main shock hypocenters are indicated by the star symbols. In both sequences, the aftershock activity occurs mainly outside of the areas of major coseismic slip.

main shock faulting (e.g., Rybicki, 1973; Aki, 1979). Such a property of aftershock faulting has important implications in the study of stress variations following main shock rupture. Additional comparisons for other earthquake sequences, however, are necessary to examine the validity of the previous observations and to further examine the mechanics of aftershock faulting.

A primary objective of this paper is to compare the distribution of aftershocks following the North Palm Springs, California, earthquake of 8 July 1986 (9:20:44 UTC) and the Borah Peak, Idaho, earthquake of 28 October 1983 (14:06:06 UTC) with their corresponding slip patterns, which have been previously derived from an inversion of digitally recorded strong-motion and teleseismic waveforms. Aftershocks of these two earthquakes were well recorded by dense local seismograph networks. In addition, we compare observed aftershock activity with main shock slip for earthquakes whose coseismic slip patterns have been previously obtained by other workers from a direct analysis of the recorded strong-motion and teleseismic data using forward-modeling techniques that attempt to fit synthetic records to the observed data.

We find that the aftershock hypocenters and fault mechanisms are consistent with a subsequent redistribution of stress following the earthquake due to increased loading away from the area of greatest moment release. Aftershocks

generally do not occur where main shock slip is large and, instead, tend to cluster near the edges of areas of maximum coseismic displacement.

Analysis

The 28 June 1966 Parkfield earthquake. Initial attempts at deriving a fault-slip distribution for the M_S 6.0 1966 Parkfield earthquake from the modeling of strong-motion data gave contradictory results (e.g., Aki, 1968; Anderson, 1974; Trifunac and Udwadia, 1974). A strong local amplification at one of the instrument sites made the overall fit to the observed data difficult and prevented the derivation of a unique slip model (Lindh and Boore, 1981). Recently, Liu (1983) has obtained a fault-slip model for the Parkfield earthquake by considering the local site effects. The slip model consists of two fault segments with right-lateral strike-slip displacement: a 22-km-long northern segment and a 10-km-long southern segment that is offset by about 1.5 km to the west. Average slip on the northern and southern segments is 45 and 21 cm, respectively (Liu, 1983). Further details of the slip distribution could not be resolved due to the poor distribution of the strong-motion instruments.

Eaton *et al.* (1970) computed hypocenters for aftershocks occurring between 1 July and 15 September using arrival-time data recorded by a dense local network of seismograph stations. We have superimposed, on the slip model of Liu (1983), the well-located aftershock hypocenters of Eaton *et al.* (1970) (see Figure 2). Although several aftershocks plot within the areas of major slip, the activity appears to form clusters near the edges or outside of those areas. Such a pattern would be consistent with the interpretation implied by the Imperial Valley and Morgan Hill results. The low resolution of the 1966 Parkfield slip pattern, however, prevents a complete evaluation of the relation between coseismic rupture and subsequent aftershock faulting.

Most of the aftershocks following the Parkfield earthquake had first-motion focal mechanisms exhibiting right-lateral strike-slip motion similar to that of

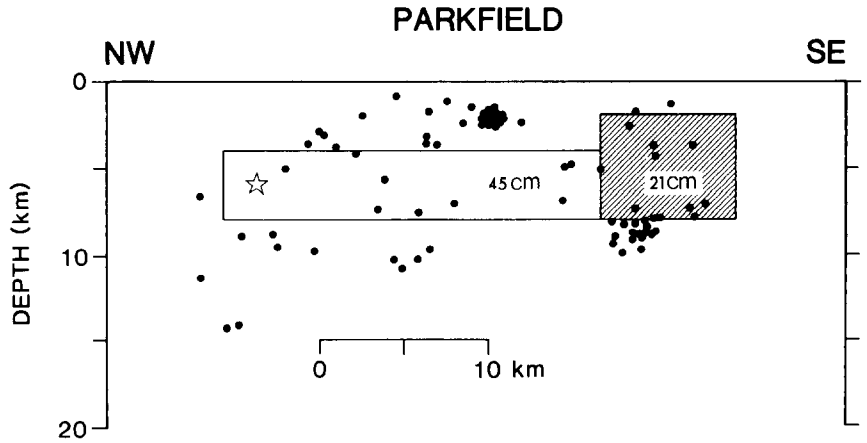

FIG. 2. Well-located aftershocks occurring within the first 2 months of the 1966 Parkfield earthquake superimposed on the fault slip model obtained by Liu (1983) for the main shock. The southern fault segment (*hachured*) is offset by 1.5 km to the west of the northern segment. Aftershocks with magnitudes greater than or equal to 1.5 are plotted (from Eaton *et al.*, 1970). Vertical and horizontal errors for these aftershocks are less than 2.5 km and generally do not exceed 1.0 km. The star denotes the main shock hypocenter.

the main shock (Eaton *et al.*, 1970). If aftershocks did not occur within the main shock source region, then these mechanisms would suggest that the aftershock activity resulted from either an expansion of the rupture on the earthquake fault or subsidiary faulting in the adjacent fault blocks along surfaces subparallel to the primary fault.

The 9 Febrary 1971 San Fernando earthquake. The rupture history of the M_S 6.6 1971 San Fernando earthquake was initially determined by Heaton and Helmberger (1979) from forward-modeling the strong ground motion records. Heaton (1982) later revised the rupture model after including teleseismic body-wave data and observed static vertical offsets in the strong-motion analysis. The revised model requires two nearly parallel thrust faults about 4 km apart. One of the fault planes corresponds to the Sierra Madre fault and dips at an angle of 54° to the north. This fault segment covers a depth range of 3 to 16 km. The second segment is south of the Sierra Madre fault and dips at a 45° angle from the surface to a depth of 8 km (see Heaton, 1982).

Prior studies of the aftershocks of the San Fernando earthquake show a crescent-shaped epicentral distribution believed to represent the main shock fault (Allen *et al.*, 1973; Whitcomb *et al.*, 1973). The initial studies attributed most of the aftershock activity to continued motion on the primary fault that had ruptured during the San Fernando earthquake. Although many aftershocks had thrust mechanisms similar to that of the main shock, numerous strike-slip and normal faulting events were also observed within the aftershock zone. Allen *et al.* (1973) suggested that left-lateral strike-slip mechanisms on the western edge of the aftershock zone implied reverse motion on a flexed surface that they interpreted to be part of the main shock fault.

Gephart and Forsyth (1984) later reexamined the aftershock data to determine the regional stress tensor. They found that the stress orientation indicated by the aftershock mechanisms fit the main shock mechanism rather poorly, suggesting that the regional stress field may have been strongly affected by the earthquake. Gephart and Forsyth (1984) also noted that the aftershock locations were more in agreement with faulting along intersecting zones of weakness, rather than on a continuous fault surface.

Figure 3 shows the San Fernando aftershocks projected on the fault-slip source model obtained by Heaton (1982) for the Sierra Madre fault segment. These aftershock locations form a large subset of the data employed by Allen *et al.* (1973) and Whitcomb *et al.* (1973) and thus maintain the same general pattern presented in the earlier studies. Many aftershocks are enclosed within the 50 cm contour of the Heaton (1982) slip model (see Figure 3). However, the majority of the aftershocks within the band of activity on the northwestern flank of the rupture area have left-lateral strike-slip mechanisms (Allen *et al.*, 1973). These mechanisms, together with the stress-field results of Gephart and Forsyth (1984), would suggest that the western activity resulted from secondary deformation within the adjoining fault blocks. Fewer aftershocks occurred on the eastern half of the rupture (see Figure 3), and these appear to be scattered away from the central portion of the region of maximum slip. These aftershocks would also project to regions outside or on the margins of the area of concentrated slip obtained by Heaton (1982) for the shallow fault segment.

The 6 August 1979 Coyote Lake earthquake. A coseismic slip model for the M_S 5.7 1979 Coyote Lake earthquake was obtained by Liu and Helmberger (1983) by also fitting synthetic records to the strong ground motion data. The distri-

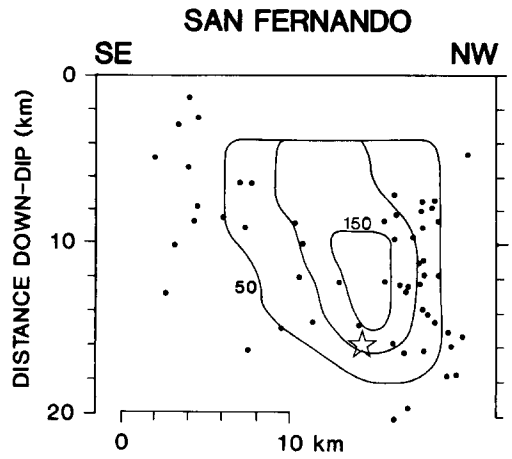

FIG. 3. Aftershock activity within the first 3 weeks following the 1971 San Fernando earthquake projected onto the main shock slip distribution obtained by Heaton (1982) for the Sierra Madre fault segment. This segment contains the main shock hypocenter (star). Slip is contoured at 50 cm intervals. Aftershocks within 5 km of the fault plane are plotted. These events have horizontal and vertical errors that do not exceed 2 and 4 km, respectively (Allen *et al.*, 1973).

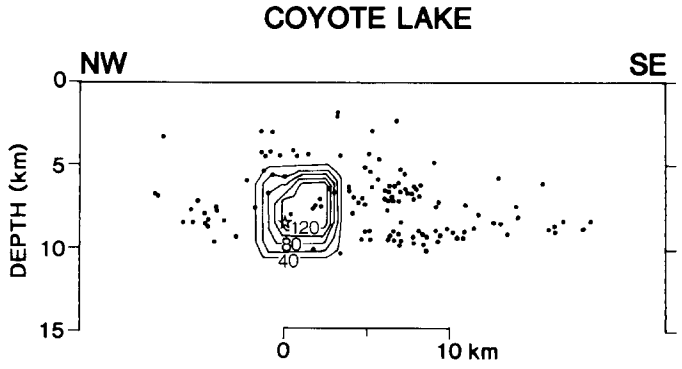

FIG. 4. Aftershocks of the 1979 Coyote Lake earthquake located by Reasenberg and Ellsworth (1982) in the vicinity of the main shock hypocenter (star) superimposed on the coseismic slip model estimated by Liu and Helmberger (1983). Twenty centimeter contours are shown for strike-slip displacement exceeding 40 cm during the main shock. Hypocentral errors for the aftershocks average less than 0.5 km (Reasenberg and Ellsworth, 1982).

bution of slip contains a single concentrated zone of right-lateral strike-slip displacement just south of the main shock hypocenter (Liu and Helmberger, 1983). We have projected aftershocks with magnitudes greater than 0.5 located by Reasenberg and Ellsworth (1982) in the vicinity of the main shock hypocenter onto the slip model of Liu and Helmberger (1983). Vertical and horizontal standard errors for these hypocenters average less than 0.5 km (Reasenberg and Ellsworth, 1982). The aftershock distribution (Figure 4) is such that most events are southeast of the region of coseismic slip. Other activity is scattered around the source area with few events occurring within the region of maximum slip identified by Liu and Helmberger (1983).

This pattern of aftershock activity surrounding a quiet region had prompted Reasenberg and Ellsworth (1982) to identify the central area as the zone of major stress release during the earthquake. Our examination of the aftershock hypocenters relative to the distribution of slip during the Coyote Lake earthquake

(Figure 4) supports their interpretation. Reasenberg and Ellsworth (1982) attributed the occurrence of the largest aftershocks at the periphery of the central quiet zone to a concentration of stress on the outer edge of the source region. First-motion focal mechanisms were computed for many of the aftershocks by Reasenberg and Ellsworth (1982). These mechanisms denote strike-slip faulting similar to that of the Coyote Lake earthquake. However, based on variations in the strike orientation, Reasenberg and Ellsworth (1982) concluded that the aftershocks occurred along multiple slip surfaces within the aftershock volume and did not reflect continuing slip on a simple planar fault surface.

The 1986 North Palm Springs earthquake. Aftershocks for the M_S 6.0 1986 North Palm Springs earthquake were well recorded by the U.S. Geological Survey–California Institute of Technology seismograph network in southern California. Preliminary locations using *P*- and *S*-phase data from the network stations indicated that aftershocks in the first 24 days after the earthquake define a broad, elliptical zone whose orientation appears to coincide with the geologically inferred geometry of the Banning fault (Jones *et al.*, 1986). Given (1986) relocated the earthquake sequence using a master-event approach; the resulting distribution of aftershock hypocenters is consistent with the pattern of Jones *et al.* (1986).

The slip distribution that we obtained for the 1986 North Palm Springs earthquake (Mendoza and Hartzell, 1988) suggests that the main shock resulted from the failure of one major localized source and another smaller region. Hartzell *et al.* (in preparation, 1988) have computed a similar slip model from an inversion of the strong motions recorded near the source. Displacement within the major sources is mostly right-lateral strike-slip with varying amounts of reverse motion. In Figure 5, we project the aftershock hypocenters relocated by Given (1986) onto

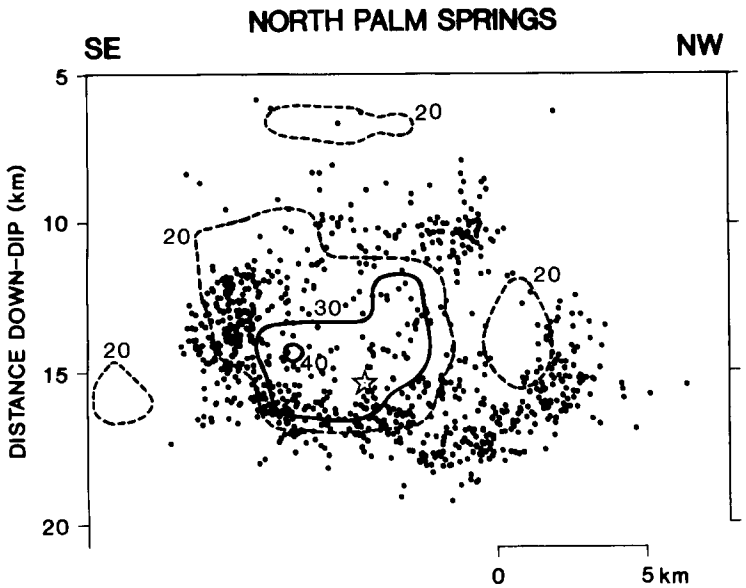

FIG. 5. Aftershocks of the North Palm Springs earthquake projected onto the fault-plane orientation used to estimate the main shock slip. Hypocentral errors for these events do not exceed 1 and 2 km in the horizontal and vertical directions, respectively (Given, 1986). Only aftershocks located within 2 km of the fault plane are plotted. Contours at 10 cm intervals are shown for strike-slip displacement exceeding 20 cm (from Hartzell *et al.*, in preparation, 1988). Relatively few aftershocks occur within the area of maximum slip (solid contour). The main shock hypocenter is indicated by a star.

the slip contours obtained by Hartzell *et al.* (in preparation, 1988). We consider only those events within 2 km of the chosen fault plane, which dips at 46° to the northeast. Most of the aftershocks relocated by Given (1986) are tightly grouped and fall within this 2 km cutoff. The aftershock hypocenters are clustered away from or near the boundaries of the area of maximum slip indicated by the strong-motion slip model. This observation is consistent with aftershocks occurring at or near the edges of the rupture due to increased stress levels following main shock faulting.

Jones *et al.* (1986) computed preliminary first-motion focal mechanisms for some of the North Palm Springs aftershocks. We have examined these mechanisms in an attempt to identify patterns in the aftershock faulting. Although most of the fault-plane solutions exhibit a nodal plane whose strike is similar to that of the Banning fault, the sense of motion on this plane varies from strike-slip to thrust. The only obvious pattern is a tendency for aftershocks with similar mechanisms to occur close together. Fault mechanisms for many more aftershocks appear to be necessary to resolve the geometry of the aftershock faults.

The 1983 Borah Peak earthquake. Several studies (Boatwright, 1985; Goter *et al.*, 1986; Richins *et al.*, 1987) have reported on the source properties of the aftershocks that followed the M_S 7.3 1983 Borah Peak earthquake. In general, the aftershock activity delineates a planar structure that appears to coincide with the main shock fault. Also, many of the aftershocks exhibit normal-faulting mechanisms similar to that of the main shock (Goter *et al.*, 1986). However, following a more detailed study, Richins *et al.* (1987) found a substantial variability in the orientation of the normal-fault mechanisms for aftershocks with magnitudes greater than 2.5 and occurring within the first 3 weeks following the main shock. They suggest that aftershock activity following the Borah Peak earthquake was mostly due to faulting along subsidiary faults. To examine the aftershocks in terms of the coseismic moment release pattern, we have projected the aftershock hypocenters computed by Goter *et al.* (1986) onto the distribution of slip obtained by Mendoza and Hartzell (1988) from the inversion of teleseismic P waveforms. The phase arrival-time data used by Goter *et al.* (1986) formed a large subset of the data used by Richins *et al.* (1987). Thus, the aftershock distributions reported in both studies are very similar.

Figure 6 shows the Borah Peak aftershocks superimposed on the main shock slip contours of Mendoza and Hartzell (1988). Only aftershocks within 5 km of the assumed fault plane, which dips 49° to the southwest, are projected. This distance includes most of the aftershock hypocenters computed by Goter *et al.* (1986). Although aftershock activity is scattered along the entire length of the rupture area, no hypocenters project to distances greater than about 15 km from the surface in the down-dip direction. This cutoff could be related to differences in stress or material properties with depth. However, the relatively narrow band of seismicity defined by the aftershock pattern appears to divide the upper and lower regions of maximum slip. Our observations of aftershock occurrence for the sequences examined earlier would suggest that this seismic activity occurred away from the regions of maximum displacement following a readjustment to the coseismic release of stress on the main shock fault.

We have examined the aftershock source mechanisms determined by Goter *et al.* (1986) from an analysis of the recorded P-wave first motions. Focal mechanisms reported for aftershocks within the upper region of large slip exhibit thrust-type motion (see Figure 6). This observation, together with the strike-slip mech-

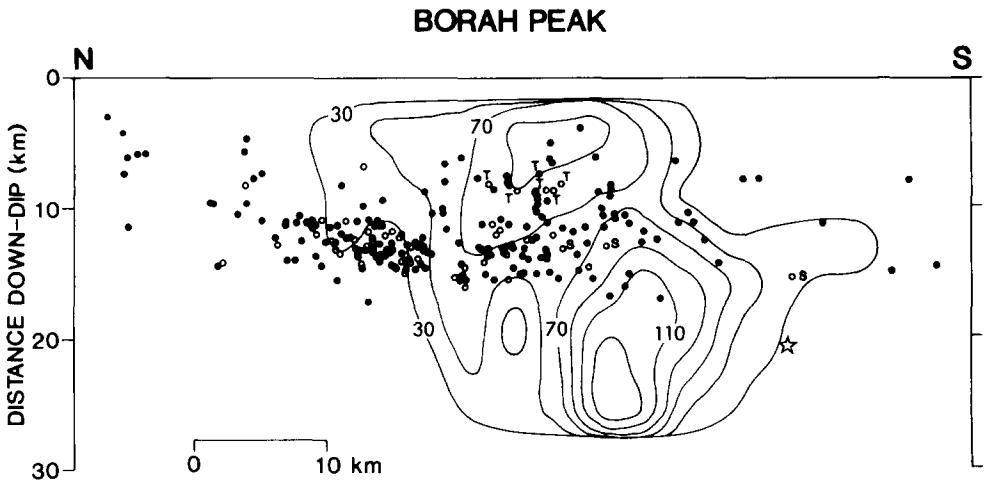

FIG. 6. Borah Peak aftershocks projected onto the dipping plane assumed by Mendoza and Hartzell (1988) for the main shock fault. Normal dip-slip motion is contoured at 20 cm intervals for areas that slipped more than 30 cm (from Mendoza and Hartzell, 1988). The figure includes only aftershocks within 5 km of the plane of projection. The maximum vertical and horizontal errors for these aftershocks are 1.6 and 2.5 km, respectively, and most do not exceed 1.5 km (Goter *et al.*, 1986). Open circles denote aftershocks whose mechanism has been computed by Goter *et al.* (1986). Thrust-fault mechanisms are labeled T, strike-slip mechanisms are labeled S, and normal-fault mechanisms are unlabeled. The star represents the main shock hypocenter.

anisms obtained for aftershocks near the deeper zone of maximum slip, support our contention that aftershocks did not occur within the areas of maximum coseismic slip. These results, which are consistent with the interpretation of Richins *et al.* (1987), imply that most of the aftershock activity within the length of the main shock rupture occurred in the adjoining fault blocks and do not reflect postseismic motion along the main shock fault.

Also apparent in Figure 6 is an intense zone of seismic activity near the northern limit of coseismic rupture. This cluster of aftershock activity is directly downdip of a bifurcation in the surface trace of the fault (see Crone *et al.*, 1987) and may reflect complicated faulting due to strain buildup north of the rupture boundary following main shock slip. Fault mechanisms determined by Goter *et al.* (1986) for aftershocks near the northern limit of coseismic rupture denote normal faulting with varying degrees of strike-slip motion. Because large uncertainties may be associated with fault-plane solutions obtained from *P*-wave first motions recorded by short-period instruments, we cannot rule out the possibility that some of the aftershocks in the cluster of activity represent continued motion at or near the main shock fault due to postseismic expansion of the slip zone.

DISCUSSION

Our comparison of aftershock patterns and distributions of coseismic slip indicates that few aftershocks occur within the areas of maximum displacement on the main shock fault, although the observation is less obvious for the 1966 Parkfield and 1971 San Fernando sequences. The data for these two sequences, however, are not as well constrained as for the more recent events.

The results are consistent with the interpretation that aftershock activity occurs in regions of concentrated stress following primary faulting during the main shock (e.g., Rybicki, 1973; Aki, 1979). The secondary seismic activity observed near the edges of the main shock slip region may result from increased stress at

the periphery of the zone of main shock faulting. Significant increases in stress are anticipated to occur at the endpoints (edges) of a single crack subjected to pure shear (e.g., Segall and Pollard, 1980; Das and Scholz, 1981). This shear-crack model, which is shown in Figure 7, also predicts a slight stress increase in a direction normal to the crack at distances greater than the crack length. Observed distributions of aftershock hypocenters for the 1968 Borrego Mountain and 1979 Homestead Valley sequences in California, and the 1972 Managua, Nicaragua, earthquake, suggest that main shock faulting may redistribute stress similarly to a shear crack (Das and Scholz, 1981; Stein and Lisowski, 1983). Most of the seismic activity following these three earthquakes appears to be restricted to regions where the shear-crack model predicts high relative stresses. The aftershock patterns examined in this study are generally consistent with this redistribution of shear stress following main shock faulting and suggest that aftershock activity is triggered in the peripheral region of the coseismic slip, either on the existing primary fault zone or within the adjoining fault blocks.

Several authors (e.g., Booker, 1974; Rice, 1980) have discussed the aftershock process following a dislocation in terms of a fluid-flow model. In this model, the total shear stress on the slipped region increases with time after the main shock rupture due to reloading by a fluid-flow process. This increase has been taken to

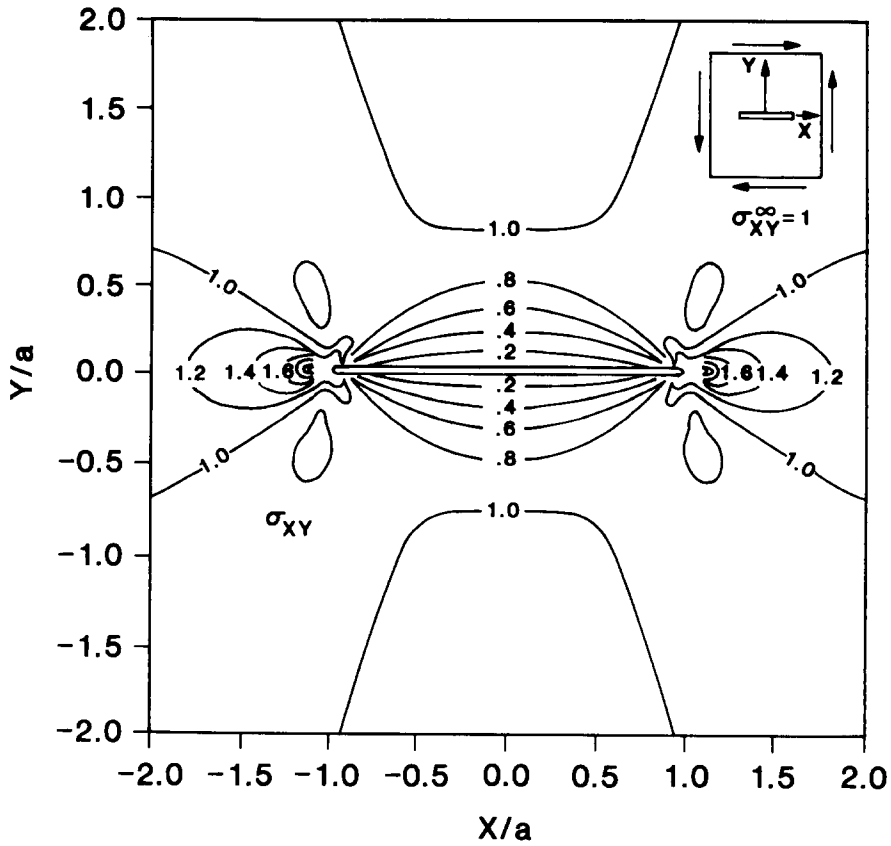

FIG. 7. Shear stress distribution around a single crack of unit length a, subjected to unit pure shear ($\sigma_{xy} = 1$) at infinity. Shear stress is symmetrical about crack center ($x = 0$) and increases significantly near the endpoints of the crack (from Segall and Pollard, 1980).

indicate that aftershocks occur on the fault surface within the region that slipped during the main shock (see Rice, 1980). Our present observations, however, preclude the triggering of aftershocks within the main shock slip region. Therefore, any increase in shear stress in the slipped region due to the flow of fluids is probably accommodated by fault creep or by secondary deformation in the surrounding volume.

Although the single crack model discussed here appears to describe the general character of the observed aftershock patterns, it greatly oversimplifies specific earthquake sequences, especially in areas of complex fault geometries where subsidiary faults of varying lengths and widths interact in a complicated manner. Major discontinuities, bends, or offsets in the ruptured fault surface would result in increased local stresses that may produce fracturing in the surrounding volume (e.g., Rybicki, 1973; Segall and Pollard, 1980). The interaction of independent fault surfaces at the right-stepping offset of the San Andreas fault near Cholame, for example, was interpreted by Segall and Pollard (1980) to result in a concentration of aftershock activity following the 1966 Parkfield earthquake. Reasenberg and Ellsworth (1982) similarly concluded that aftershocks following the 1979 Coyote Lake earthquake resulted from a redistribution of local stresses due to the interaction between a complex network of primary and secondary faults.

Observed patterns of aftershock activity probably reflect a more complicated distribution of stress that depends on the crustal structure and on the interaction of the main shock rupture zone with preexisting subsidiary faults or zones of weakness in the surrounding volume. Rybicki (1973) has shown that the stress field produced by main shock faulting can be significantly perturbed both by the free surface and by layering in the geologic structure. Rice and Gu (1983) discuss the response of secondary faults to coseismic stress changes and suggest that activation of these faults following large earthquakes may be aided by relaxation processes at depth. Restressing of the near-surface volume may occur due to aseismic slip at depth or to relaxation of the asthenosphere or lower crust (Rice and Gu, 1983). A more appropriate mechanical model of aftershock occurrence is needed that would incorporate the influence of the free surface and crustal layers, the triggering mechanisms outlined by Rice and Gu (1983), and the clustering properties observed in this study.

The results of this investigation may have implications in the study of seismicity patterns. The observations indicate that aftershock patterns can be helpful in locating earthquake source areas, as suggested by several authors from qualitative examinations of aftershock locations (e.g., Reasenberg and Ellsworth, 1982; Bakun *et al.*, 1986; Cockerham and Eaton, 1987). However, not all areas of decreased aftershock activity may correspond to main shock slip zones, and some care must be exercised when inferring the distribution of slip for a particular earthquake solely from the observed distribution of aftershock locations.

Another point is the apparent discrepancy between aftershock patterns observed after large earthquakes at subducting plate boundaries and those observed to follow large events in other tectonic environments. Many large shallow subduction earthquakes are immediately followed by aftershock sequences that exhibit a strong clustering behavior. These aftershock clusters have frequently been interpreted to represent localized zones of increased strength or stress on the plate interface (e.g., Valdes *et al.*, 1982; Mendoza and Dewey, 1984; Chatelain *et al.*, 1986). The zones, sometimes termed barriers or asperities, may denote interplate patches whose rupture recurs through time, producing similar earth-

quakes for successive earthquake cycles. Our present results would indicate that clustering would occur near the edges, rather than within the asperity zones. More complete studies of main shock–aftershock patterns should probably be conducted for subduction regions prior to making inferences about interplate properties from the observed distribution of postseismic activity.

Acknowledgments

Susan Goter and Doug Given kindly provided their hypocentral data for the Borah Peak and North Palm Springs aftershocks. Comments by Bill Stuart, Rob Cockerham, and an anonymous reviewer greatly improved the manuscript.

References

Aki, K. (1968). Seismic displacements near a fault, *J. Geophys. Res.* **73,** 5359–5376.

Aki, K. (1979). Characterization of barriers on an earthquake fault, *J. Geophys. Res.* **84,** 6140–6148.

Allen, C. R., T. C. Hanks, and J. H. Whitcomb (1973). San Fernando earthquake: seismological studies and their tectonic implications, in *San Fernando, California, Earthquake of February 9, 1971,* Vol. III, U.S. Government Printing Office, Washington, D.C., 13–21.

Anderson, J. (1974). A dislocation model for the Parkfield earthquake, *Bull. Seism. Soc. Am.* **64,** 671–686.

Bakun, W. H., G. C. P. King, and R. S. Cockerham (1986). Seismic slip, aseismic slip, and the mechanics of repeating earthquakes on the Calaveras fault, California, *Earthquake Source Mechanics, Geophysical Monograph 37,* American Geophysical Union, 195–207.

Boatwright, J. (1985). Characteristics of the aftershock sequence of the Borah Peak, Idaho, earthquake determined from digital recordings of the events, *Bull. Seism. Soc. Am.* **75,** 1265–1284.

Booker, J. R. (1974). Time dependent strain following faulting of a porous medium, *J. Geophys. Res.* **79,** 2037–2044.

Chatelain, J. L., B. L. Isacks, R. K. Cardwell, R. Prévot, and M. Bevis (1986). Patterns of seismicity associated with asperities in the central New Hebrides island arc, *J. Geophys. Res.* **91,** 12497–12519.

Cockerham, R. S. and J. P. Eaton (1987). The earthquake and its aftershocks, April 24 through September 30, 1984, in *The Morgan Hill, California Earthquake of April 24, 1984,* S. N. Hoose, Editor, *U.S. Geol. Surv. Bull. 1639,* 15–28.

Crone, A. J., M. N. Machette, M. G. Bonilla, J. J. Lienkaemper, K. L. Pierce, W. E. Scott, and R. C. Bucknam (1987). Surface faulting accompanying the Borah Peak earthquake and segmentation of the Lost River fault, central Idaho, *Bull. Seism. Soc. Am.* **77,** 739–770.

Das, S. and C. H. Scholz (1981). Off-fault aftershock clusters caused by a shear stress increase? *Bull. Seism. Soc. Am.* **71,** 1669–1675.

Doser, D. I. and H. Kanamori (1986). Depth of seismicity in the Imperial Valley region (1977–1983) and its relationship to heat flow, crustal structure, and the October 15, 1979, earthquake, *J. Geophys. Res.* **91,** 675–688.

Eaton, J. P., M. E. O'Neill, and J. N. Murdock (1970). Aftershocks of the 1966 Parkfield-Cholame, California, earthquake: a detailed study, *Bull. Seism. Soc. Am.* **60,** 1151–1197.

Gephart J. W. and D. W. Forsyth (1984). An improved method for determining the regional stress tensor using earthquake focal mechanism data: application to the San Fernando earthquake sequence, *J. Geophys. Res.* **89,** 9305–9320.

Given, D. D. (1986). Master event relocations of the North Palm Springs earthquake sequence of July 1986 (abstract), *EOS, Trans. Am. Geophys. Union* **67,** 1089.

Goter, S. K., W. D. Richins, and C. J. Langer (1986). Aftershocks of the Borah Peak, Idaho, earthquake of 28 October 1983: catalog of locations and single-event focal mechanisms, *U.S. Geol. Surv., Open-File Rept. 86-277.*

Hartzell, S. H. and T. H. Heaton (1983). Inversion of strong ground motion and teleseismic waveform data for the fault rupture history of the 1979 Imperial Valley, California, earthquake, *Bull. Seism. Soc. Am.* **73,** 1553–1583.

Hartzell, S. H. and T. H. Heaton (1986). Rupture history of the 1984 Morgan Hill, California, earthquake from the inversion of strong motion records, *Bull. Seism. Soc. Am.* **76,** 649–674.

Heaton, T. H. (1982). The 1971 San Fernando earthquake: a double event?, *Bull. Seism. Soc. Am.* **72,** 2037–2062.

Heaton, T. H. and D. V. Helmberger (1979). Generalized ray models of the San Fernando earthquake, *Bull. Seism. Soc. Am.* **69,** 1311–1341.

Jones, L. M., L. K. Hutton, D. D. Given, and C. R. Allen (1986). The North Palm Springs, California earthquake sequence of July 1986, *Bull. Seism. Soc. Am.* **76,** 1830–1837.

King, G. C. P., Z. X. Ouyang, P. Papadimitriou, A. Deschamps, J. Gagnepain, G. Houseman, J. A. Jackson, C. Soufleris, and J. Virieux (1985). The evolution of the Gulf of Corinth (Greece): an aftershock study of the 1981 earthquakes, *Geophys. J. R. Astr. Soc.* **80,** 677–693.

Lindh, A. G. and D. M. Boore (1981). Control of rupture fault geometry during the 1966 Parkfield earthquake, *Bull. Seism. Soc. Am.* **71,** 95–116.

Liu, H.-L. (1983). Interpretation of near-source ground motion and implications, *Ph.D. Thesis,* California Institute of Technology, Pasadena, California, 184 pp.

Liu, H.-L. and D. V. Helmberger (1983). The near-source ground motion of the 6 August 1979 Coyote Lake, California, earthquake, *Bull. Seism. Soc. Am.* **73,** 201–218.

Mendoza, C. and J. W. Dewey (1984). Seismicity associated wiith the great Colombia-Ecuador earthquakes of 1942, 1958, and 1979: implications for barrier models of earthquake rupture, *Bull. Seism. Soc. Am.* **74,** 577–593.

Mendoza, C. and S. H. Hartzell (1988). Inversion for slip distribution using teleseismic *P* waveforms: North Palm Springs, Borah Peak, and Michoacan earthquakes, *Bull. Seism. Soc. Am.* **78,** 1092–1111.

Reasenberg, P. and W. L. Ellsworth (1982). Aftershocks of the Coyote Lake, California, earthquake of August 6, 1979: a detailed study, *J. Geophys. Res.* **87,** 10637–10655.

Rice, J. R. (1980). The mechanics of earthquake rupture, in *Physics of the Earth's Interior,* A. M. Dziewonski and E. Boschi, Editors, North-Holland Publishing Co., Amsterdam, The Netherlands, 555–649.

Rice, J. R. and J.-C. Gu (1983). Earthquake aftereffects and triggered seismic phenomena, *Pure Appl. Geophys.* **121,** 187–219.

Richins, W. D., J. C. Pechmann, R. B. Smith, C. J. Langer, S. K. Goter, J. E. Zollweg, and J. J. King (1987). The 1983 Borah Peak, Idaho, earthquake and its aftershocks, *Bull. Seism. Soc. Am.* **77,** 694–723.

Rybicki, K. (1973). Analysis of aftershocks on the basis of dislocation theory, *Phys. Earth. Planet. Interiors* **7,** 409–422.

Savage, M. K. and R. P. Meyer (1985). Aftershocks of an $M = 4.2$ earthquake in Hawaii and comparison with long-term studies of the same volume, *Bull. Seism. Soc. Am.* **75,** 759–777.

Segall, P. and D. D. Pollard (1980). Mechanics of discontinuous faults, *J. Geophys. Res.* **85,** 4337–4350.

Stein, R. S. and M. Lisowski (1983). The 1979 Homestead Valley earthquake sequence, California: control of aftershocks and postseismic deformation, *J. Geophys. Res.* **88,** 6477–6490.

Trifunac, M. D. and F. E. Udwadia (1974). Parkfield, California earthquake of June 27, 1966: a three-dimensional moving dislocation, *Bull. Seism. Soc. Am.* **64,** 511–534.

Valdes, C., R. P. Meyer, R. Zuniga, J. Havskov, and S. K. Singh (1982). Analysis of the Petatlan aftershocks: numbers, energy release, and asperities, *J. Geophys. Res.* **87,** 8519–8527.

Whitcomb, J. H., C. R. Allen, J. D. Garmany, and J. A. Hileman (1973). San Fernando earthquake series, 1971: focal mechanisms and tectonics, *Rev. Geophys. Space Phys.* **11,** 693–730.

U.S. GEOLOGICAL SURVEY
NATIONAL EARTHQUAKE INFORMATION CENTER
BOX 25046, MS 967
DENVER, COLORADO 80225 (C.M.)

U.S. GEOLOGICAL SURVEY
SEISMOLOGICAL LABORATORY (252-21)
CALIFORNIA INSTITUTE OF TECHNOLOGY
PASADENA, CALIFORNIA 91125 (S.H.H.)

Manuscript received 3 November 1987